22

Femtosecond Fabrication of Waveguides in Ion-Doped Laser Crystals

Andrey Okhrimchuk
Fiber Optics Research Center of RAS
Russian Federation

1. Introduction

Permanent refractive index change (PRICE) in dielectrics by means of the femtosecond laser pulses is a novel enabling technology in photonics. A wide range of photonic structures manufactured using this method has been demonstrated in glasses and crystals since the first observation of the underling phenomenon (Davis, 1996). While numerous waveguides, waveguide lasers and amplifiers, couplers and Bragg gratings were fabricated on the basis of this phenomenon, PRICE theory is far from accomplishment yet, although some basic principles are beyond any doubt. To date it is obvious that to understand femtosecond modification of a transparent dielectric the process should be separated in two stages. The first stage consists of the non-linear absorption of a femtosecond pulse and electron plasma generation. The second stage consists of energy transfer from the electron plasma to ions and structural changes in a dielectric. The first stage seems to be very analogous both in glasses and crystals, as it deals with electronic excitation and only material parameters required for its description are energy gap width and coefficients of multiphonon absorption (MPA).
The second stage still rises many questions and should be considered as an incomplete chapter in PRICE theory. To date it is not clear whether PRICE proceeds in the same manner both in crystals and glasses. It is generally understood for glasses and associated with melting and densification (Glezer, 1997; Streltsov & Borelli, 2001). As a rule it gives positive refractive index change in the exposed region, and its magnitude can be as high as 10^{-2} (Allsop, 2010). Thus a straightforward way for waveguide inscription is open for glasses.
Contrary to glasses PRICE is rather more complicated and intrigued in crystals. As a rule refractive index change is negative in the exposed region. For example, a widely accepted point of view relays on the assumption that a crystal undergoes amorphisation in the exposed region, and this causes stresses and positive refractive index change in the surrounding area (Gorelik, 2003; Apostolopoulos, 2004). Thus a waveguide is usually created in the area adjacent to tracks written by femtosecond beam. Since in this case waveguiding is due to an indirect effect accompanying femtosecond modification of crystal lattice, magnitude of refractive index change in the waveguide is not so high as in glass waveguides and does not exceed $1*10^{-3}$ (Nejadmalayeri, 2005; Torchia, 2008; Siebenmorgen, 2009; Silva, 2010; Bookey, 2007; Burghoff, 2007). This value is not enough to build compact waveguide lasers with diode pumping. Meantime in many cases crystals are more a attractive media for femtosecond fabrication of compact waveguide lasers in comparison to glasses, because they have better thermo-conductivity, high optical damage threshold and

allow high doping level of rare-earth and transition metal ions without significant degradation of spectroscopic characteristics. Finally negative refractive index change could be altered to an advantage, as it allows writing a cladding, while a waveguide core is composed of unperturbed crystal region. In such architecture degradation of spectroscopic parameter is excluded and scattering loss is basically lower.
This paper is devoted to investigation of the processes relating to femtosecond writing of waveguides in laser crystals doped by rare-earth and transition metal ions, as well as to design and fabrication of crystalline waveguide lasers. The author proposes his own point of view on processes taking place in crystal, and methods for inscription of low loss waveguides in ion-doped YAG crystals. An example of a waveguide laser will be presented.

2. Waveguide fabrication technique and architecture

Numerous femtosecond lasers operating in NIR (Ti: sapphire or Yb-based lasers) or VIS (harmonic of Ti:sapphire laser), and even in Mid-IR (OPO, 2400 nm) are used for waveguide fabrication in transparent dielectrics. They are either oscillators providing pulses with high rep rate from range of 5 MHz to 25 MHz, or regenerative amplifiers providing lower rep rate nearly less than 5 MHz. A sample is mounted on high-precision 3-D translation stage, and laser beam is tightly focused in the sample volume at a depth of 20-500 μm under polished surface of the sample. Microscopic lenses with numerical aperture NA= 0.4 – 1.4 are usually used for focusing, providing beam waist as low as 0.5 - 2 μm. Focusing depth is first of all constrained by aberrations which a converging beam suffered at air-dielectric interface (they could be reduced by implementing immersion liquid). Another constrain is the lens working distance. While the sample is moving in the direction perpendicular to the laser beam, beam waist produces a permanent stable track of modified material with altered refractive index, or permanent refractive index change (PRICE). Velocity of the translation in dependency of laser rep rate may be in the range of 0.01 – 50 mm/s.
Under moderate pulse energy, suitable for waveguide fabrication, PRICE is positive in fused silica and most of glasses (Davis, 1996; Miura, 1997; Homoelle, 1999; Schaffer, 2001; Streltsov, 2001). Thus even a single track recorded in glass is a waveguide core, while surrounding area is a cladding (Fig.1a). Transverse cross section of such waveguide is generally elliptical. Ellipticity is high for low rep rate inscription. Special beam shaping is applied in order to make waveguide with a circular cross section at low rep rate laser systems (Osellame, 2003; Moh, 2005; Marshall, 2006). High rep rate lasers provide circular waveguide cross section even without beam shaping due to strong cumulative heating effect (Eaton, 2005). However it holds true for glasses with low thermal conductivity (borosilicate, boroaluminosilicate, etc.), and does not work for fused silica.
Situation is more complicated in crystals. Positive refractive index change in the exposed crystal area was observed only under certain restricted conditions. Refractive index change is positive in $LiNbO_3$ crystal for extraordinary axis under low pulse energy (Burghoff, 2006; Burghoff, 2007). Second harmonic generation in a waveguide written in this regime in z-cut PPLN crystal was demonstrated (Lee, 2006). A track has a pronounced elliptical cross section with width of about 1 μm and was elongated in direction of femtosecond beam propagation by 10 μm and more. Because of this a multiscan technique was applied in order to fabricate a more symmetrical waveguide core. That is, 6 tracks separated by 0.7 μm in direction perpendicular to a track and beam propagation were written (Fig.1b). A near-circular single mode waveguide of analogous type was fabricated in z-cut $LiNbO_3$ single crystal (Bookey, 2007). In this work the modified region of the crystal is consisted of two

parts: rectangular damaged region and a waveguide of 8.9 μm x 21 μm cross section underneath the damaged region (Fig.1c).

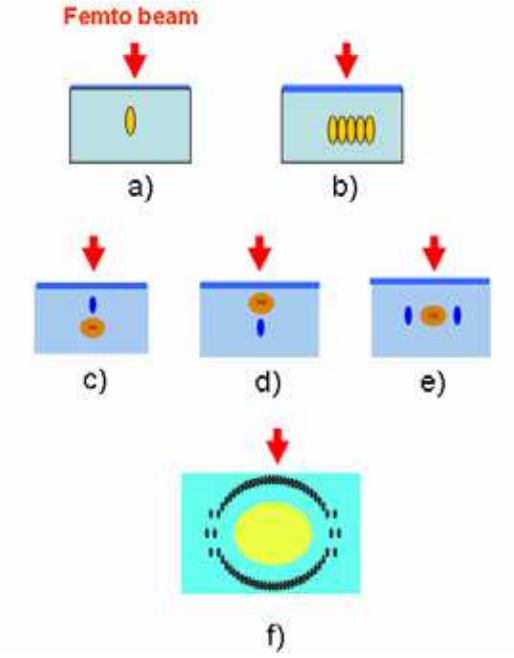

Fig. 1. Architectures of femtosecond written waveguides. Direct writing of a core: a) a single track, b) a multiple track core. Stress induced waveguides: c) and d) a waveguide is below and above the track, e) waveguide is in between two tracks. f) A micro-structured depressed cladding waveguide.

Sign of PRICE induced by 11-MHz rep rate Ti-Sapphire oscillator in YAG:Cr^{4+} crystal depends upon speed of crystal translation and pulse energy (Okhrimchuk, 2008). In Fig.2 the waveguide written in the regime of positive PRICE with a high aperture focusing lens (NA=0.8) is presented. The waveguide core of a rectangular 35x55 μm cross-section consistes of 30 parallel tracks separated in horizontal and vertical transverse dimensions by 3.5 and 20 μm correspondingly. Refractive index profile of the waveguide recorded by QPm technique (http://www.iatia.com.au) under observation in the direction of femtosecond laser beam propagation is shown in Fig.3.

The 1 kHz Ti:Sapphire laser always produces a negative PRICE in YAG single crystals (Okhrimchuk, 2005-a, 2005-b; Siebenmorgen, 2009). It was reported that in the ceramic YAG doped with 2 at.% of Nd^{3+} ions PRICE is negative too (Torchia, 2008). However there is refractive index increase in the area closely adjacent to a track (Dubov, 2004; Siebenmorgen, 2009) that is due to elasto-optical effect. The waveguide is produced due to this phenomenon in these works. An advanced waveguide architecture consists of two parallel tracks separated by 15 – 25 μm inscribed with a 1 kHz rep rate lasers (Fig. 1e). Although PRICE is negative inside tracks, mechanical stress induced between them provides positive PRICE. This way a single mode waveguide with almost circle mode profile was manufactured both in single

Fig. 2. End view of a waveguide written by Ti-Sapphire oscillator operating at 11-MHz rep rate. The arrow indicates direction of the femtosecond beam.

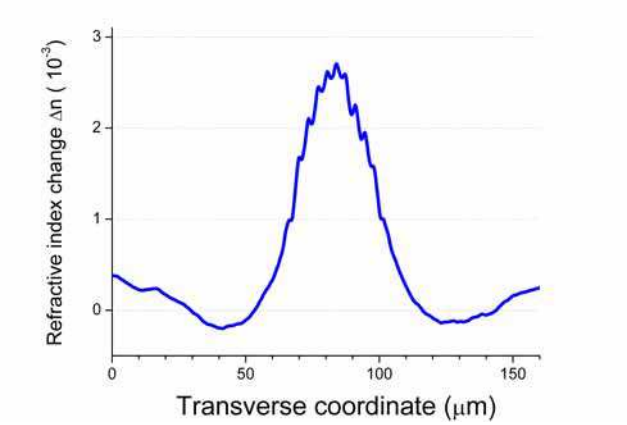

Fig. 3. Refractive index profile of a waveguide presented in Fig.2.

crystal and in ceramic YAG (Torchia, 2008; Siebenmorgen, 2009). In this design waveguide core is the stressed area which is not exposed by the femtosecond beam. An identical scheme was implemented earlier in x-cut $LiNbO_3$ single crystal (Burghoff, 2006), and z-cut PPLN (Thomas, 2007) and then in YVO_4:Nd single crystal (Silva, 2010).

Refractive index alteration was found in Al_2O_3:Ti^{3+} single crystal under irradiation with 1 kHz rep rate Ti:sapphire laser. PRICE is negative inside a track analogously to YAG crystal, and a waveguide arises in the area below or above the track (Apostolopoulos, 2004) (Fig.1 c,d). No refractive index change was observed in Al_2O_3:Ti^{3+} under irradiation with a high rep rate laser.

Waveguide fabrication in crystalline silicon was made by irradiation at wavelength of 2400 nm with OPO pumped by chirped-pulse-amplified mode-locked Ti:sapphire laser (Nejadmalayeri,

2005). Plate of crystalline silicon was coved by oxide layer of 20 μm thickness. Femtosecond beam was focused inside silicon through this layer. An inscribed track produces mechanical stress, which causes index increase in the restricted area located between the track and silica-silicon interface. This way a waveguide with strong birefringence was fabricated.
An original approach based on negative PRICE was proposed by the author (Okhrimchuk, 2005-a; Okhrimchuk, 2009). A single mode and multimode waveguides were fabricated with a depressed cladding in YAG:Nd (1 at.%), YAG:Cr^{4+}, diffusion bonded YAG:Nd/YAG:Cr^{4+} and YAG:Yb(15 at.%) crystals. A femtosecond laser beam from a Ti-sapphire laser system operating at 800 nm with 1 kHz repetition rate (Spitfire, Spectra Physics) was used for waveguides fabrication. The laser produced pulses with 115 fs pulse width (FWHM). A

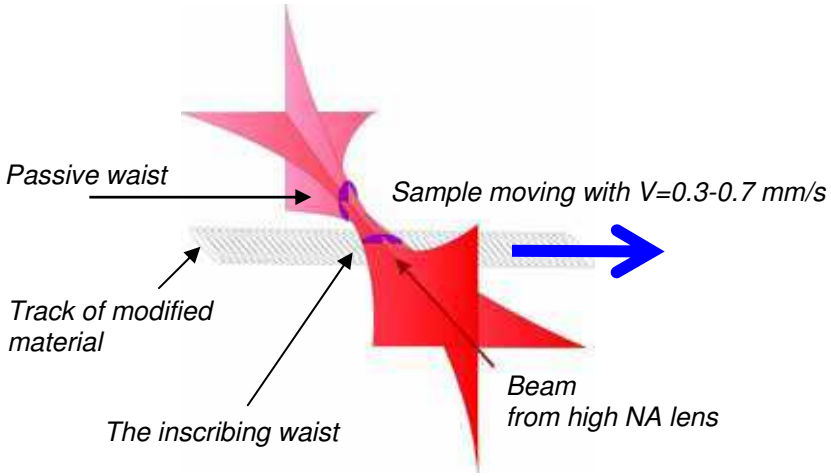

Fig. 3. Focusing of femtosecond beam with an elliptical cross section.

crystal sample was placed on a high precision 3-D Aerotech translation stage. Laser beam was focused under the crystal surface with Carl Zeiss (NA=0.65) or Mitutoyo lens (NA = 0.55). The crystal was translated at a constant speed of 0.3 - 0.7 mm/s to inscribe smooth tracks with lowered refractive index. A femtosecond laser beam with elliptic cross-section was used for the inscription. It proves to produce much more homogeneous tracks in YAG crystals compared to a standard beam of circular cross-section (Okhrimchuk, 2009). Such an approach leads to a dramatic reduction of scattering loss. To achieve this, a plane-concave cylindrical lens was placed before the high aperture lens to produce a waist of elliptical cross-section. Normally, two elliptical waists with mutually orthogonal orientations of principal axes were formed with ratio of major to minor diameters of nearly 10 (Fig.3). Typically, more than a half of input pulse energy was absorbed in the first waist nearest to the focusing lens. Therefore, for the moderate input energies used in the experiments, the inscription threshold was not reached in the second waist. Thus, tracks were inscribed by the first waist having a principal axis parallel to an inscribing track.
An elemental structural unit (a track) was produced by straight moving of the crystal with constant velocity so that a femtosecond beam waist crosses crystal from one edge to another. Cross section of a track is close to an oval with large to small axes ratio being larger then 10. In dependency on crystal doping it has refractive index lowered by $(1 - 5)\times10^{-3}$ in comparison with unperturbed value in the bulk of crystal, thus tracks all together formed a

waveguide cladding, while a core corresponded to a non-perturbed region of the crystal (Fig.1-f). Author would like to stress that a waveguide is formed due to lowed refractive index in the cladding. Unlike to alternative design with one or two tracks (Fig.1 c,d,e), author considers that contribution of mechanical stress in the core is negligible for this method of inscription and waveguide architecture.

Basing on the above approach a rectangular shaped, 10 mm long waveguide with core dimensions of 100 μm x13 μm was fabricated in YAG:Nd^{3+} (0.8 at.%) as shown in Fig. 5. (Okhrimchuk, 2005-a). Propagation loss for the fundamental mode was estimated to be as low as 0.2 dB/cm at wavelength of 1064 nm.

Single mode waveguide with mode field size comparable with standard Yb-doped fiber was fabricated in YAG:Cr^{4+} crystal (Okhrimchuk, 2009-b). End view of this waveguide is shown in Fig.6. It works as a waveguide saturable absorber insuring Q-switch operation of an Yb-fiber laser.

Multimode waveguides efficiently guiding light of multimode high power laser diodes were inscribed in diffusion bonded YAG:Nd/YAG:Cr^{4+} and YAG:Yb(15 at.%) crystals. (Fig.7 & 8). The tracks were written perpendicular the YAG:Nd/YAG:Cr^{4+} interface plane, thus waveguide crossed the bonded crystal from its Nd-part to Cr-part. Total number of tracks creating cladding equals 66 for both crystals. Numerical mode analysis of the waveguide shown in fig.7 was performed with a commercial code (www.comsol.com). The electromagnetic eigenvalue problem was solved by the finite-element method. It was found

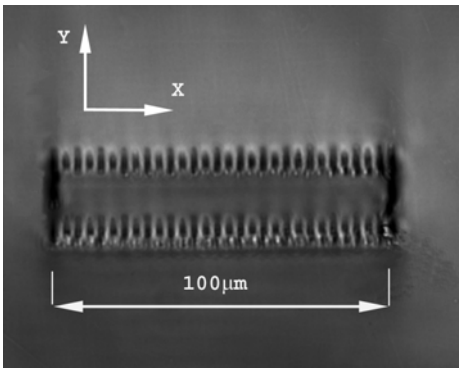

Fig. 5. End view of a depressed cladding waveguide inscribed in YAG:Nd^{3+}.

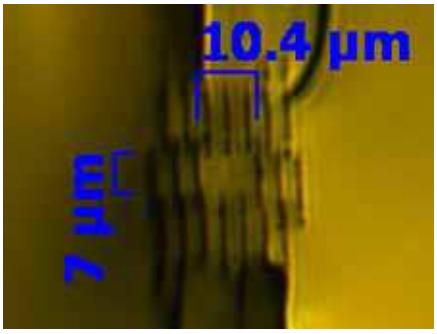

Fig. 6. End view of a depressed cladding waveguide inscribed in YAG:Cr^{4+}

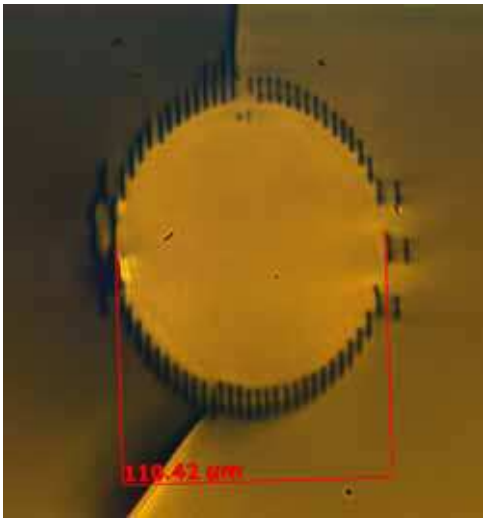

Fig. 7. End view of a depressed cladding multimode waveguide inscribed in diffusion bonded YAG:Nd/YAG:Cr^{4+} crystal. The refractive index is lowered by nearly 3×10^{-3} in each track compared to the unperturbed value in the bulk of crystal.

That the structure maintains 24 leakage modes at wavelength of 1064 nm. The propagation loss for two fundamental modes with mutually orthogonal polarisations was derived from the imaginary part of the propagation constant, and was determined to be less then $4\cdot10^{-3}$ cm^{-1}. It was experimentally found that both waveguides are strong enough to keep pump emission in the waveguide core (Fig.9 & 22). Finally an efficient Q-switch operation was obtained in YAG:Nd/YAG:Cr^{4+} crystal (see chapter 6).

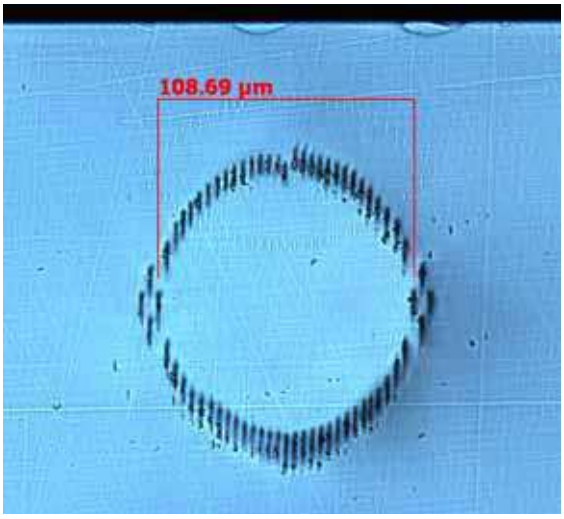

Fig. 8. End view of a depressed cladding waveguide inscribed in YAG:Yb^{3+}

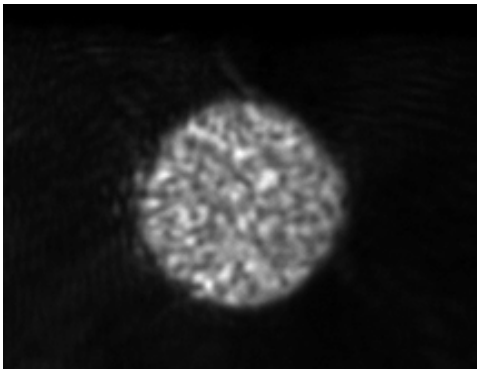

Fig. 9. Near field image of pump light at the output of the waveguide in YAG:Yb shown in Fig.8.

Propagation attenuation for pump emission in the waveguide inscribed in YAG:Yb crystal was measured in dependency upon numerical aperture (NA) of the input pump light at 965 nm. Experimental setup for measurement is shown in Fig.10. The total pump attenuation in the waveguide was found to be 5 cm^{-1} for pumping light with NA≤0.09, while absorption coefficient due Yb^{3+} ions is as high as 3.5 cm^{-1}. Thus ratio of bulk absorption coefficient of the crystal to the total waveguide propagation attenuation coefficient is as high as 0.7 for input light cone corresponding to NA=0.09. Thus pump should be efficiently utilized in the waveguide.

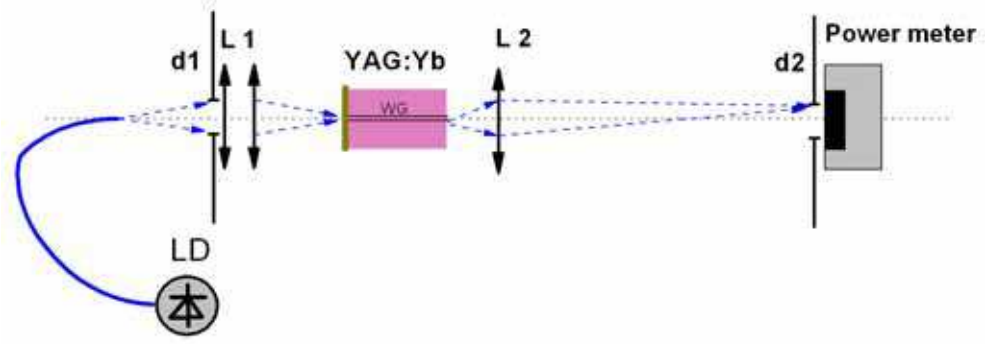

Fig. 10. Experimental setup for pump light attenuation measurements.

3. Grating inscription in YAG crystals

Two techniques of Bragg gratings inscription were tested both at fundamental wavelength of the femtosecond laser system (800 nm), and at the second harmonic (400 nm). First technique is a direct "point-by-point" (P-by-P), and the second is based on beam intensity modulation by Quartz acoustic modulator (AOM) (2008, Marshall). Differential interference contrast microscopy (DIC) was applied for inscribed structures inspection.

It was reasonably expected that a minimal inscribable grating pitch would be of the order or even slightly lower than a wavelength of a femtosecond laser due to sufficiently non-linear character of light-matter interaction. This consideration was supported by grating inscription in fused silica, where smallest grating with pitch of 260 nm was obtained by P-

by-P technique with beam wavelength of 800 nm (Dubov, 2006;). However it was found in the course of grating inscription experiments that grating pitch in YAG crystals can not be inscribed smaller than 800 nm even with inscribing beam wavelength of 400 nm. When author tried to write grating with pitch size smaller than 800 nm, chaotic overcoming of grating marks was obtained. Microscopic pictures of gratings with minimal inscribable pitches for different inscription regimes are shown in Fig. 11 for inscription wavelength of 800 nm and in Fig.12, 13 for the wavelength of 400 nm.
The expected pitch size should be calculated by formula:

$$\Delta = \frac{V}{f}, \tag{1}$$

where V is sample moving velocity, and f is whether laser repetition rate, or AOM modulation frequency in dependency of technique applied. The inscribed grating pitch size obeys formula (1) when P-by-P technique was applied under moving velocity V=0.8 mm/s or higher and pitch size of 800 nm or higher is obtained (Fig.11 a,b), and no gratings were inscribed when V<0.8 mm/s. Analogous behaviour was observed for AOM modulation technique. For example, when we tried to inscribe pitch of Δ=410 nm a grating of nearly double size than predicted by formula (1) was really obtained (Fig.11- c).
It was a surprise that the smallest inscribable pitch size was found to be around 900 nm for femtosecond beam wavelength of 400 nm and P-by-P technique, and this pitch size is even larger, than for beam wavelength of 800 nm. It is interesting that a refractive index structuring was found when crystal was very slowly moving so that according formula (1) Δ<100 nm (Fig.12). Moreover nearly the same period of refractive index modulation of 900 nm was obtained. These facts coerce to suppose that some self-organising processes take place in this case.
Attempts were made to inscribe gratings with pitches sizes of Δ= 410, 670 and 760 nm under AOM modulation at wavelength of 400 nm. Instead gratings with nearly the same pitch sizes of 1100 – 1200 nm were really obtained (Fig.13).
Obtained experimental results open possibility for 1-st order Bragg grating writing for wavelength of 2.9 μm (2nΔ), which are promising for fabrication of waveguide Er:YAG lasers.

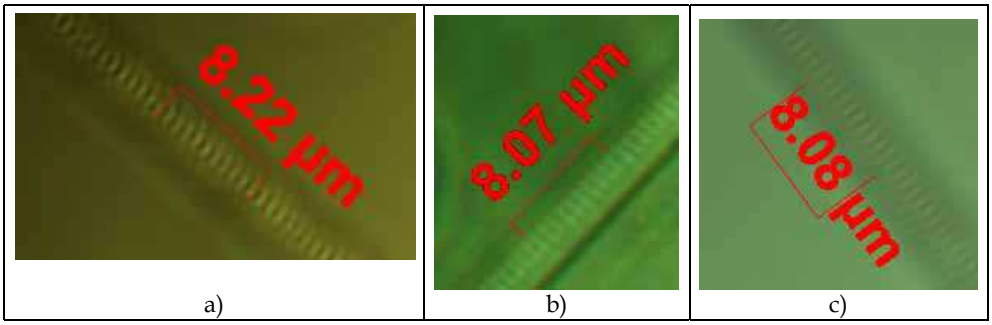

Fig. 11. Gratings inscribed in YAG:Cr^{4+} crystal at wavelength of 800 nm with point-by-point technique (a,b) and AOM modulation (c):
(a) beam of a circular cross section; V=0.80 mm/s; f=1 kHz, E_{in}=0.2 μJ.
(b)beam of an elliptical cross-section; V=0.81 mm/s; f=1 kHz, E_{in}=1.1 μJ.
(c) beam of an elliptical cross-section; V=0.0094 mm/s; f=23 Hz, E_{in}=1.8 μJ

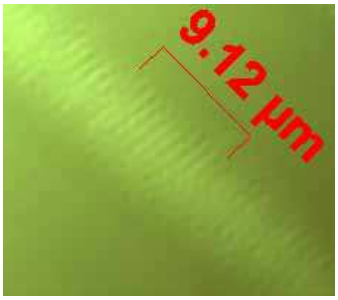

Fig. 12. Self-organised gratings inscribed in YAG:Cr^{4+} crystal at wavelength of 400 nm with slow moving (V<0.015 mm/c).

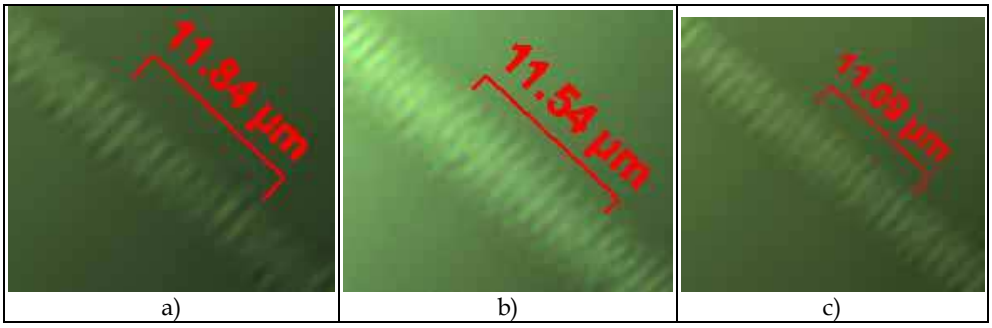

Fig. 13. Gratings inscribed in YAG:Cr^{4+} crystal at wavelength of 400 nm by AOM modulation technique with beam of an elliptical cross-section; E_{in}=0.56 μJ:
(a) f=23 Hz, V=0.0094 mm/s;
(b)f=23 Hz, V=0.0154 mm/s
(c) f=23 Hz, V=0.0174 mm/s.

4. Non-linear interaction of a femtosecond laser beam with dielectrics.

There are no doubt that understanding of processes concerning interaction of femtosecond pulses with a crystal lattice plays a central role in successful advancement of the technology. The first stage of this interaction comprising non-linear absorption of femtosecond pulses is rather clear and described in details in literature. This description is common for crystals and glasses, and even liquids (for wideband dielectrics).
It is a widely accepted that the process of energy absorption dealing with material modification by pulses shorter than 1 ps is determined by i) multi-photon absorption and ii) resistive heating of the generated plasma. These processes can be mathematically described by a popular simplified model for the evolution of the scalar electric field envelope $A(x,y,z,t)$ in paraxial approximation and electron density $\rho(x,y,z,t)$. Although the paraxial approximation has certain restrictions in exact quantitative description of femtosecond beam propagation dealing with practically used conditions of beam focusing (a high NA lens is generally used), it helps to understand basic character and peculiarities of the process, and to get a qualitative visual at least. It comprises nonlinear partial differential equations that account for the major propagation effects such as diffraction, Kerr nonlinearity, group

velocity dispersion, multi-photon absorption, impact ionization and absorption and defocusing by the generated electron-hole plasma (Feng, 1997, Berge, 2007; Turitsyn, 2007):

$$i\frac{\partial A}{\partial z}+\frac{1}{2k}\left(\frac{\partial^2}{\partial x^2}+\frac{\partial^2}{\partial y^2}\right)A-\frac{k''}{2}\frac{\partial^2 A}{\partial t^2}+k_0 n_2\left|A\right|^2 A=-\frac{i\sigma_{bs}}{2}(1+i\omega\tau_e)\rho A-\frac{i\beta_K}{2}\left|A\right|^{2K-2}A \quad (2a)$$

$$\frac{\partial\rho}{\partial t}=\frac{1}{n^2}\frac{\sigma_{bs}}{E_g}\rho\left|A\right|^2+\frac{\beta_K}{K\hbar\omega}\left|A\right|^{2K} \quad (2b)$$

The last three terms in the left-hand side of Eq.(2a) describe effects of beam diffraction, group velocity dispersion (GVD), and Kerr nonlinearity, respectively. The latter term alone is responsible for a catastrophic self-focusing which is limited by the effects described by terms on the right-hand side of Eq.(2a), namely plasma absorption and defocusing, and multi-photon absorption. In Eq.(2a) the laser beam propagation along the z axis is assumed and this equation is essentially a reduced paraxial approximation of the wave equation for the complex electric field envelope A with a carrier frequency ω in the moving frame of coordinates. $k= nk_0= n\omega/c$ is the propagation vector, n is the material linear refraction index, k'' is the GVD parameter, n_2 is the nonlinear refractive index describing Kerr effect, σ_{bs} is the cross section for inverse Bremsstrahlung, τ_e is the electron-phonon collision time in conduction band, and the quantity β_K describes the K-photon absorption ($K>1$). Equation (2b) implements the simplest Drude model for electron-hole plasma in dielectrics and describes the evolution of the electron density ρ. The first term on the right-hand of eq. (2b) side is responsible for the avalanche impact ionization and the second term – for the ionization resulting from multi-photon absorption (MPA). E_g is the energy gap between valence and conduction bands.

Self-focusing dealing with Kerr non-linearity plays an essential role in the inscription process. This role is obviously destructive for smart modification of crystal, and apparently it can play a positive role in some cases for inscription of structures in glasses of sub-wavelength sizes (Dubov, 2006). Self-focusing leads to filamentation and fragmentation of a laser beam and this is a one course of scattering loss in waveguides written in this regime. Authors of (Turitsyn, 2007) discussed regimes of inscription with a diminishing role of self-focusing. As a result of theoretical analysis they offered to use a non-Gaussian ring-shaped beam in order to increase self-focusing threshold, while PRICE threshold remains unchanged.

In the work (Okhrimchuk, 2009-a) beam of elliptical cross-section is suggested as a tool diminishing the self-focusing. A negative cylindrical lens with large focal length was arranged in the femtosecond beam path before it passes to the focusing lens. It is considered that breaking of axial symmetry of the beam postpones self-focusing to higher input energies, which partly takes place without the cylindrical lens. Self-focusing easily deforms axially-symmetric beam profile in such a way that the central (part) core of the beam suffers from spatial collapse caused by non-linear focusing. The collapsed part could be effectively absorbed, thus PRICE threshold is reached in this small central part, while the rest of the beam exhibits loss-less propagation. When a cylindrical lens is inserted, PRICE threshold is reached in wider area of beam cross-section, and the beam experiences a more uniform absorption, which decreases a transmittance, as it was observed in experiment (Table.1). This result suggests that breaking of axial symmetry of the femtosecond beam is a promising technological method to prevent destructive self-focusing at small energies, and thus it may

lead to a better control over the energy deposition and a waveguides inscription process. The track made with the cylindrical lens is smooth, without any observable defects. Such tracks form a depressed cladding waveguide as it was demonstrated (Okhrimchuk, 2005-a, 2009-b).
Understanding of relative contribution of the MPA the MPA and the plasma absorption and the plasma absorption in the process of energy deposition leading to PRICE is ultimately required for optimization of the inscription process. Transmittance of laser crystal and glasses in dependency on input p*u*lse energy was measured with this purpose (Okhrimchuk, 2009-a). Focusing conditions in these experiments were identical to conditions of waveguide inscription. Ti:sapphire oscillator-amplifier with repetition rate was of 1 kHz was used in these experiments. PRICE threshold was measured in the same conditions too (Table.1).

Material	MPA order K (λ, nm)	MPA coefficient β_K,	w/o cyl. lens E_{in} (nJ)			Transmittance at the threshold	
			Inscription thresholds	with cyl. lens E_{in} (nJ).	Intensity threshold, (10^{13} W/cm^2) (with & w/o cyl. Lens)	w/o cyl. lens.	with cyl. lens
YAG	**5** (800)	$3.1 \cdot 10^{-51}$ cm^7/W^4	61	610	**4.8**	0.64	0.49
YAG:Nd^{3+}			55	580	**4.5**	0.66	0.54
YAG:Cr^{4+}	(800)		46	1200	**4…9**		
	(400)		50	500			
$RbPb_2Cl_5$:Dy^{3+}				90	**0.66**		
ZnSe:Cr^{2+}			10^4		**850**		
ZnSe (polycr.)	**2**		n/r	n/r		-	-
ZnS:Cr^{2+} (polycr.)	**2**		250*	n/r up to 7000			
ZnS:Cr^{1+} (polycr.)	**2**		1250*				
Fused silica	**5**	$1.2 \cdot 10^{-51}$ cm^7/W^4	55	460	**3.6**	0.83	
	6	$2.7 \cdot 10^{-65}$ cm^9/W^5					
BK7	**3**	$2.7 \cdot 10^{-24}$ cm^3/W^2	55	550	**4.4**	0.71	0.55
	4	$6.9 \cdot 10^{-38}$ cm^5/W^3					
	5	$1.9 \cdot 10^{-51}$ cm^7/W^4					

Table 1. Result of measurement of the non-linear transmittance in dependency upon input pulse energy and the inscription thresholds. n/r - threshold is not reached for the investigated input energy range.

It is instructive to present the results of the transmittance experiments in terms of the absorbed pulse energy versus input energy in double logarithmic coordinates as shown in Fig. 14 for the beam of circular cross section and in Fig15 for the beam of elliptical cross section. Very similar dependences for the transmittance and values of threshold input energes were obtained for undoped YAG, YAG:Nd^{3+}, YAG:Cr^{4+} crystals, fused silica and BK7 glass. Strongly difference dependence was found for ZnSe crystals, and inscription threshold is not reached at all in range of input energies investigated.

Different behaviour is seen for the absorption in YAG crystals for low and high energy regions. It is natural to assume that different mechanisms are responsible for absorption in these regions. It is well established that for 100 fs pulse width and moderate electric field strength the non-linear absorption in wide band insulators is initiated by MPA process (Berge, 2007; Turitsyn, 2007). Following this it is reasonable to consider MPA process dominates in the low energy region, while the plasma absorption prevails for higher energies. Confirmative results were obtained while investigating electronic excitations in SiO_2, Al_2O_3 and MgO crystal by measurement of induced phase shift of a delayed probe beam (Quere, 2001). They found a transition from MPA absorption regime to free carrier absorption at the input pulse intensity nearly corresponding to the dependence curve bend in Fig. 14 &15. As phase shift saturates authors of the last paper consider that there is no more electronic density rise for input intensities higher than 10^{14} W/cm^{2,} and the electronic avalanche process is an ineffective in comparison with MPA. This is completely in agreement with a tendency of the absorption curve to be linear for high input pulse energies (Fig.14 &15).

So as MPA is dominant in non-linear absorption up to inscription threshold , and it is a main channel of supplying a conduction band by electrons, we can estimate free electron concentration at the threshold and above as:

$$\rho = \frac{\Delta E_{abs}}{E_g V_m}, \tag{3}$$

E_g is the energy gap, where $\boldsymbol{\Delta E_{abs}}$ is energy absorbed due to MPA at the threshold, $\boldsymbol{V_m}$ is volume occupied by free electrons. It is reasonably to consider that region occupied by free electrons is converted to the modified region (region of PRICE), and these regions nearly coincide with each other. Sizes of PRICE region were directly measured with a microscope: $\boldsymbol{V_m}$= 1μm x10μm x 12μm = 1.2*10^{-10} cm^2 for YAG:Nd(0.5%) crystal modified in the setup with the cylindrical lens. $\boldsymbol{\Delta E_{abs}}$= 0.04 μJ as could be defined from fig.15. Finally we obtain for free electron density $\boldsymbol{\rho}$= 3*10^{20} cm^{-3}.

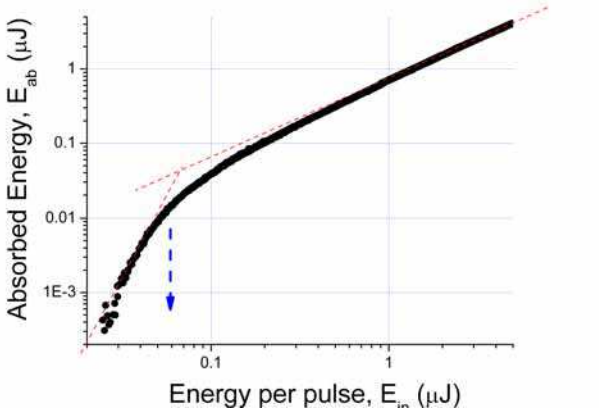

Fig. 14. Dependence of pulse absorbed energy in undoped YAG crystal in dependency upon input pulse energy. The arrow indicates PRICE threshold. Inscribing beam has cross section of circular symmetry.

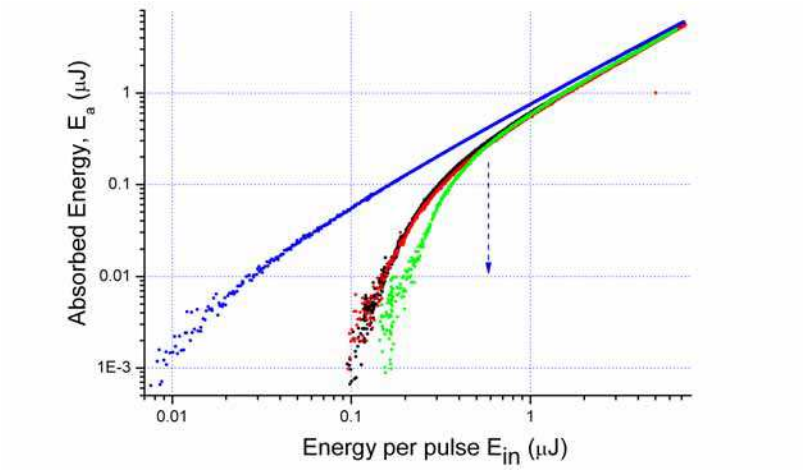

Fig. 15. Dependence of pulse absorbed energy in undoped YAG and YAG:Nd(0.5%) crystals (black and red points correspondingly) ZnSe crystal (blue points) and BK7 glass (green points) in dependency upon input pulse energy. The arrow indicates PRICE threshold for YAG and BK7. Inscribing beam has cross section of an elliptical symmetry.

Under approximations of Drude electron plasma density can be related with high frequency relative permittivity by following formula (Ashcroft & Mermin, 1976; Martin, 1997):

$$\varepsilon(\omega) = \varepsilon_c - \frac{4\pi\tau_e{}^2 e^2 \rho}{m_{eff}(1+\omega^2\tau_e{}^2)} + i\frac{4\pi\tau_e e^2\rho}{m_{eff}\omega(1+\omega^2\tau_e{}^2)}, \tag{4}$$

where ε_c is permittivity of unexcited crystal, m_{eff} is effective electron mass. Absorption coefficient of free electrons a is defined by imaginary part of permittivity:

$$\alpha = \frac{4\pi\tau_e e^2\rho}{m_{eff} nc(1+\omega^2\tau_e{}^2)}, \tag{5}$$

where c is speed of light. The experimental transmittance data gives estimation of free electron absorption coefficient a as high as 1000 cm^{-1}. Now we can estimate with formula (5) free electron time τ_e. Accepting the effective mass equalled to an electron mass m_e we find a reasonable value τ_e= 2 fs. Thus it confirms correctness of our previous estimations of free electron density ρ and a determinative role of MPA in generation of free electrons in conduction band. Parameters concerned inscription in YAG are summarised in table 2.

Free electron density ρ	$3*10^{20}$ cm^{-3}
Free electron time τ_e	2 fs
Effective electron mass, m_{eff}	m_e
Plasma absorption coefficient, a	1000 cm^{-1}
MPA coefficient β_5,	$3.1 \cdot 10^{-51}$ cm^7/W^4

Table 2. Material parameters concerned femtosecond inscription in YAG crystals.

Experimental transmittance data in the low energy region can be described analytically under conditions of smallness of the loss terms in the right hand side of Eq. (2a) and sub-critical propagation regime when the peak pulse power is lower than the critical value for self-focusing (Okhrimchuk, 2009-a). These assumptions justify self-similar quasi-linear approximation for pulse propagation (Turitsyn, 2007). Self-similar Gaussian shape of the pulse is a good approximation. Under this simplification the following analytical formula for transmittance $T(E_{in})$ corresponding to pure MPA absorption can be derived:

$$T(E_{in}) = \left(1 + (K-1)a(K)E^{K-1}\right)^{-\frac{1}{K-1}}$$
$$\alpha(K) = \beta_K \cdot \left(\frac{2}{\pi}\right)^{3/2\cdot(K-1)} \cdot \frac{\pi \cdot \mu(K) \cdot n}{K^{3/2} \cdot \lambda \cdot \tau_p^{K-1}} \cdot \frac{1}{\omega_0^{2\cdot(K-2)}}, \qquad (6)$$
$$K = \{2,3,4,5,6\}, \quad \mu(K) = \pi \cdot \left\{1, \frac{1}{2}, \frac{3}{8}, \frac{5}{16}, \frac{35}{128}\right\}$$

where λ is a central wavelength, $2\tau_p$ is laser pulse width at $1/e^2$. Applicability of the formula (6) is not limited to low energy region. In fact, it describes MPA for wider range of transmittance, if the beam remains its Gaussian shape. The restriction of formula (6) arises from plasma related absorption and beam defocusing. The dependences for transmittance measured for un-doped YAG crystal, fused silica and BK7 glass were fitted with formula (6) (Okhrimchuk, 2009-a). The only fitting parameters were the order of MPA K, coefficient of MPA β_K. Results of fitting are summarised in Table 1.

5. Nature of refractive index change in YAG crystals.

Dependence of PRICE upon input pulse energy was investigated at wavelength of 800 nm at the experimental setups designed for waveguide inscription (see chapter 2). Two different setups were used: the first is based on a high rep rate oscillator (11MHz), and the second setup comprises a low rep rate oscillator – regenerative amplifier system (1 kHz).

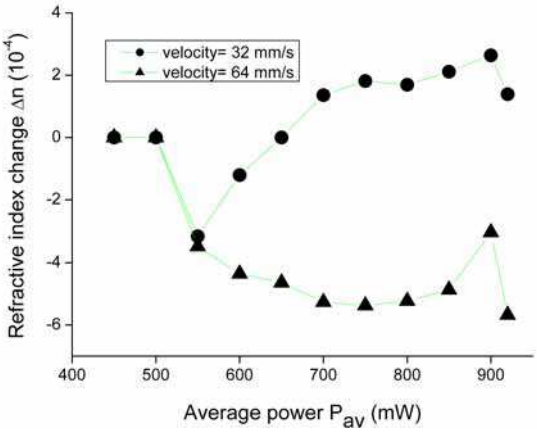

Fig. 16. Dependencies of PRICE and track height in YAG:Cr^{4+} crystal upon average input power. 11 MHz rep rate femtosecond laser.

Sign of PRICE induced by 11-MHz rep rate Ti-Sapphire oscillator in YAG:Cr^{4+} crystal depends upon speed of crystal translation and pulse energy (Okhrimchuk, 2008). For example at velocity V=32 mm/s it is positive for pulse energy exceeding 50 nJ, and is negative for pulse energies ranging from PRICE threshold to 50 nJ (Fig. 16).
Setup with 1 kHz laser includes Mitutoyo lens and a negative cylindrical lens with focal lens of 34 cm. The beam was focused at the depth of 60 μm. Translation speed was of 0.5 mm/s. Series of tracks written under different input pulse energies was inscribed. End view of a typical track is shown in Fig.17. Refractive index profiles of tracks were measured my QPm method at wavelength of 605 nm (http://www.iatia.com.au). PRICE is always negative for 1 kHz rep rate laser system. Typical index profile is shown in Fig17. Both PRICE magnitude and height of the track depend upon the input pulse energy, corresponding dependences for YAG:Nd(0.3 at.%) crystal are shown in Fig.18.

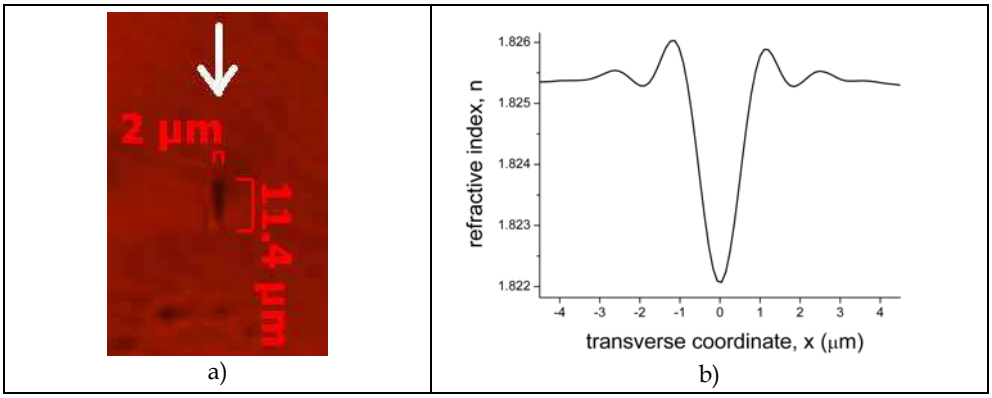

Fig. 17. a) Microscopic end view of a track inscribed in YAG:Nd(0.3%) crystal at a depth of 60 μm. b) Refractive index profile of the same track. The arrow indicates the direction of the femtosecond beam and of observation when index profile was measured.

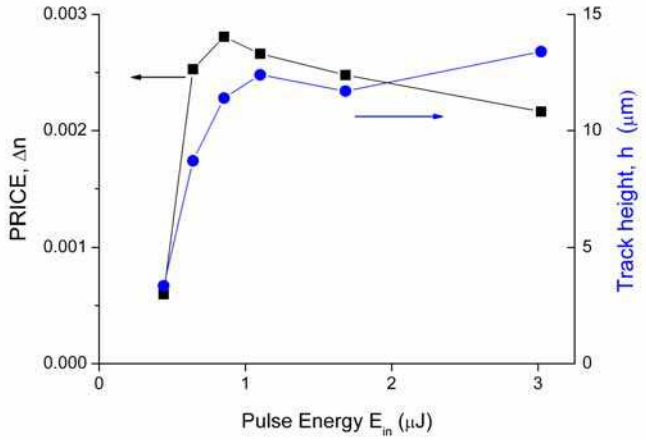

Fig. 18. Dependencies of PRICE and track height in YAG:Nd(0.3%) crystal upon input pulse energy.

Similar dependencies were found for YAG:Nd and YAG:Cr crystals. Dependence of refractive index change upon pulse energy has strong threshold character, and it saturates when the pulse energy exceeds the threshold by nearly factor of two. The saturation level depends upon doping level. Fig. 19 shows a dependence of the index change amplitude on the total concentration of dopant ions the crystal, measured for fixed input energy of 1 μJ. At this level of exposure refractive index change in a normally undoped YAG crystal strongly varied from sample to sample, and probably is determined by real purity of the crystal. Fig.19 includes data for one of the undoped YAG crystal investigated only, which probably has highest quality.

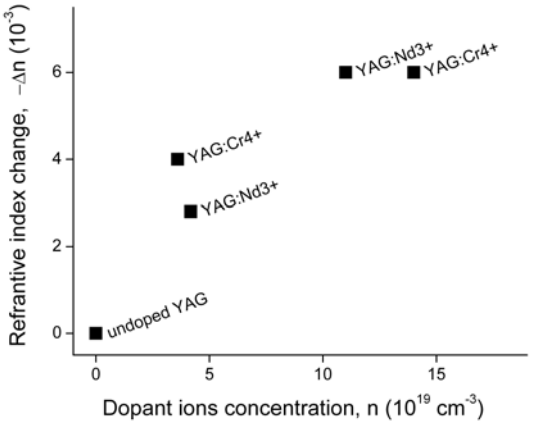

Fig. 19. Dependence of PRICE upon total dopant concentration in YAG crystal under input pulse energy of inscription of 1 μJ.

Reflectance spectrum of the modified region of the YAG:Nd crystal was investigated (Okhrimchuk, 2005-b). A rectangular area of 2000x2000 μm inside a crystal volume was processed by a focused femtosecond laser beam by writing a number of parallel tracks, inscribed with a spacing of 3 μm and laying in one plane. The beam was focused by microscope objective with NA=0.65 at a depth of 200 μm under the crystal surface and had intensity of 0.5 PW/cm^2 in focus. The thickness (height) of the modified volume was approximately 10 μm. Then unexposed layer of material between the exposed volume and the surface was removed by polishing. As a result, the processed volume of material could be directly accessed and characterised.

Reflectance spectra corresponding to the vibration modes of the crystal were recorded by using a standard FTIR spectrophotometer (Bruker, model Vector-22), customised for the measurements of reflected signals. The reflection spectra, measured with a resolution of 2 cm^{-1} are presented in Fig.20.

Firstly, the general profile of the spectrum corresponding to the exposed material is very similar to that of the unprocessed material, indicating that the garnet crystal lattice remains intact after ultrafast laser exposure. At the same time the spectrum lines of the processed material exhibit a shift to higher frequency which non-uniformly varies with frequency and shows a tendency to increase at higher frequencies. The maximal frequency shift equals 5 cm^{-1} approximately. Therefore, one can state that processing by an ultrafast laser causes a positive shift in vibration frequencies of YAG:Nd lattice. The above measurement of positive shift in vibration frequencies is in line with the negative change of refractive index, observed

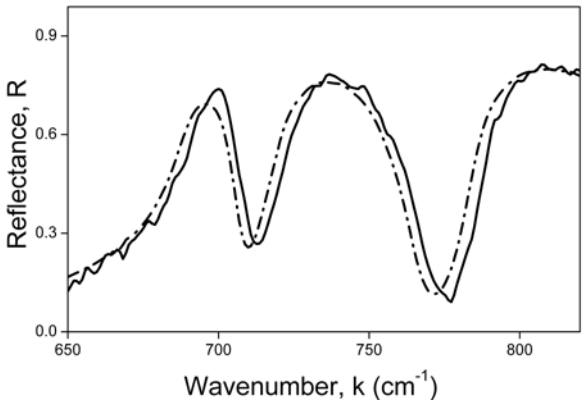

Fig. 20. Reflectance spectra of exposed (solid line) and unexposed (dashed-dotted line) of the YAG:Nd crystal.

earlier in phase delay measurements. Indeed, according to the Kramers-Kronig analysis, dielectric susceptibility $\boldsymbol{\varepsilon} = \boldsymbol{\varepsilon}' + \boldsymbol{i}\cdot\boldsymbol{\varepsilon}''$ in the region of transparency could be estimated as (Landay & Lifshits, 1982):

$$\varepsilon(\omega) = a - \frac{b}{\omega^2}$$
$$b = \frac{2}{\pi}\int_0^{\omega_1} x\varepsilon''(x) \tag{7}$$

where $\boldsymbol{a}$ – constant, $\boldsymbol{\omega_1}$ – cut-off frequency of vibration band. Results of the spectral measurements indicate that integral $\boldsymbol{b}$ increases in the processed material as a result of the general positive frequency shift in the vibration spectrum. For the refractive index change $\boldsymbol{dn}$, one can obtain from (7):

$$dn = d\sqrt{\varepsilon} = -db\cdot\frac{1}{2\omega\sqrt{a\omega^2 - b}} < 0 \tag{8}$$

Unchanged state of the reflectance spectrum indicates that notwithstanding a widely spreading hypnosis of melting the mechanism of YAG crystal modification under low repetition rate exposition differs from those taking place in glasses and crystalline quartz (Gorelik, 2003). The following simple estimation of crystal heating under exposition by one femtosecond pulse supports this statement. Temperature rise due to absorbed energy can be estimated under assumption that there are no channels of heat dissipation outside of electron plasma region:

$$\Delta T = \frac{\Delta E_{abs}}{c_p \rho_{YAG} V_m} \tag{9}$$

Accepting c_p= 0.84 J/K (T=900 K), ρ_{YAG}=4.5 g/cm^3, V_m= 1.2*10^{-10} cm^3 (see chapter 4), we obtain that ΔT= 1300 K. Such temperature rise is not enough for YAG melting (T_m= 2220 K).

Moreover, if one takes into account energy loss due to irradiation, an estimation of temperature change even decreases. Definitely that temperature rise plays a higher role in the case of the high repetition rate inscription (Fig. 16.). However a luminescence spectrum of Cr^{4+} ions recorded in the regime of guiding of pump and luminescence emission does not differ from those recorded for unperturbed crystal area (Okhrimchuk, 2008). This fact excludes any amorphisation of YAG crystal for the high repetition rate inscription too.

Another mechanisms excluding melting should be found to explain PRICE in YAG crystal. It is evident from the results presented in Fig. 19 that reaction of YAG crystals to the femtosecond laser irradiation strongly depends upon concentration of defects in the crystal. This can be explained by the assumption that the point defects existing in the crystal define the possibility of modification of YAG crystal lattices without optical damage, resulting in the well-defined refractive index change. Such behavior arises from phenomenon that dopants present in a YAG crystal generate several types of lattice defects, and its concentration is rather higher, than in an undoped crystal. These defects interact with crystal lattice and each other and form a system with week binding. The flexible defect system of a doped crystal readily reacts to moderate external perturbation such as a high-intensity optical pulse, unlike regular ions of a crystal. Thus modifications without crystal lattice destroy can take place for some restricted range of pulse energies. There are no room for similar changes in ideal crystals and its modification probably occurs in a form of crystal lattice destroy only. The defect system has remarkable contribution to dielectric susceptibility of the crystal. Modification of the defect system is accompanied by changing of dielectric susceptibility of a crystal which manifests itself, in particular, as a change of the refractive index.

Recent investigation of some femto exposed complex glasses by means of electron probe microanalyzer (EPMA) (Kanehira, 2008; Liu, 2009) and electron dispersive x-ray spectroscopy (Liu, 2008) have revealed migration of positive ions out of an exposed region, while oxygen ions concentrate inside this region. Author of these papers explain the effect by temperature diffusion. Although temperature rise should have strong effect on ion mobility, let us to suppose another explanation. Diffusion expansion of electron plasma can be a driving force for ions migration. Indeed, average electron velocity in the conduction band can be calculated accordingly (Ashcroft & Mermin, 1976):

$$V_e = \frac{e|A|}{m_{eff}\omega} \tag{10}$$

Under pulse energy of 1 μJ, we get $V_e \approx 1.5 * 10^8$ cm/s. Average diffusion length of a free electron before its trapping by a hole or a lattice defect is calculated by the formula:

$$\langle l_e \rangle = V_e \sqrt{2\tau_e t_{tr}} \tag{11}$$

where t_{tr} is the electron trapping time. The last parameter was measured for Al_2O_3 and SiO_2 crystals (Guizard, 1995). It was found to be about 100 ps in Al_2O_3. So as chemical bonds in Al_2O_3 and in YAG crystals are similar we can accept this value for estimation of the average diffusion length in YAG. Taking into account τ_e=2 fs (table 2) we obtain $\langle l_e \rangle$= 1 μm. Thus increase of electron plasma cloud size is comparable with its initial size. This could explain the reason of impossibility of inscription grating pitch smaller that 800 nm (chapter 3). The expanding electron plasma could drag some weekly bonded positive ions outside the

exposed area. In this case even inscription with a shorter wavelength does not reduce a minimal inscribable pitch, because minimal pitch size not defined by size of the exposed area, but by size of the electron plasma expanding for a long time after laser pulse is over. Accordingly to this assumption another situation should take place in SiO_2, as electron trapping time is found to be rather shorter in this material (150 fs). Thus electrons is trapped very quickly and there are no plasma expansion. This is in line with successful inscription of a very small pitch in fused silica (Dubov, 2006).

The model of electron plasma dragging ions explains positive effect of implementation of the cylindrical lens (Okhrimchuk, 2009-a). When the lens is used the electron plasma cloud has a shape of a flattened ellipsoid, and a normal to its surface is primary directed perpendicular to direction of an inscribed track. Thus each pulse drags ions predominantly outside area of modification. This is not the case for beam of circular cross section, when remarkable part of ions are pushed in the direction of the track, and each following pulse redistributes ions arranged by previous one. This could provoke instabilities in the track writing process. On the contrary pulses push ions in the same direction, when the cylindrical lens is applied. In other words, beam of an elliptical cross-section works as an "optical plug".

6. Microchip waveguide laser operating in Q-switch mode

In this chapter an example of successful application of the femtosecond inscription technology is presented. A waveguide was fabricated with a depressed cladding in a diffusion bonded YAG:Nd^{3+}/YAG:Cr^{4+} crystal under a crystal surface at 110 μm depth (for an optical axis of the waveguide). The YAG:Nd^{3+} and YAG:Cr^{4+} crystals were diffusion bonded at high temperature close to the melting point. Concentration of Nd^{3+} ions was 1 at.%. The calcium co-doping was used to switch valence of chromium to 4+. An absorption coefficient in the YAG:Cr^{4+} crystal at 1064 nm was of 4 cm^{-1}. The experimental setup for waveguide inscription is described in chapter 2. Cross section of a track is close to an oval with large to small axes ratio being more than 10. The refractive index was lowered by nearly 3×10^{-3} compared to the unperturbed value in the bulk of crystal. As a result, the array of tracks formed a waveguide cladding, while a core was corresponded to a non-perturbed region of the crystal.

Crystal surfaces with the waveguide ends have been polished, and dielectric coating was applied in order to complete a laser cavity. The neodymium end was provided with a diachronic mirror reflecting 100% at 1064 nm and transmitting 98% at 808 nm. An output coupler (OC) with the reflection coefficient of 65% at 1064 nm was made at the chromium end. Small signal transmittance of YAG:Cr^{4+} crystal was of 57 %. The total waveguide length was of 5.4 mm; length of the neodymium part was of 4 mm. Microscopic image of the waveguide end view is shown in Fig 7.

The scheme of laser setup is shown in Fig. 21. In this design a pump power is delivered from a laser diode (Lumics) through the fiber of NA=0.15 and core diameter of 105 μm. Pump fiber core diameter is only slightly lower than the waveguide laser core diameter (110 μm). It was found the waveguide is strong enough to keep pump emission at the waveguide core. Near field image of OC end is taken for pump power below Q-switch oscillation threshold (Fig.22), thus it corresponds to pump emission only. Diameter of the pump emission spot exactly matches to diameter of the waveguide core. No sufficient leakage of pump is observed (small leakage is noticed on the right side that corresponds to discontinuity in the waveguide

cladding). Oscillation was investigated in a pulsed pump mode with repetition rate ranging from 1 Hz to 10 kHz and pump pulse duration of 100 – 250 μs. Q-switch pulse energy and duration were found to be independent upon repetition rate. At repetition rate of 1 kHz and pump pulse duration of 250 μs output pulse energy is as high as 10 μJ, and threshold pump energy is 200 μJ (pump power is 0.85 W). It is important to note that nearly 3-times larger pump energy is required to produce the same output energy in traditional bulk microchip laser without waveguide but with the same other parameters (the OC and YAG:Cr^{4+} transmittances, the cavity length). Time profile of the Q-switch pulse posses a single pick shape without any additional shoulder at the pulse tail for investigated repetition rates (Fig 23). Pulse duration was found to be 1 ns (FWHM) for entire investigated repetition rate range.

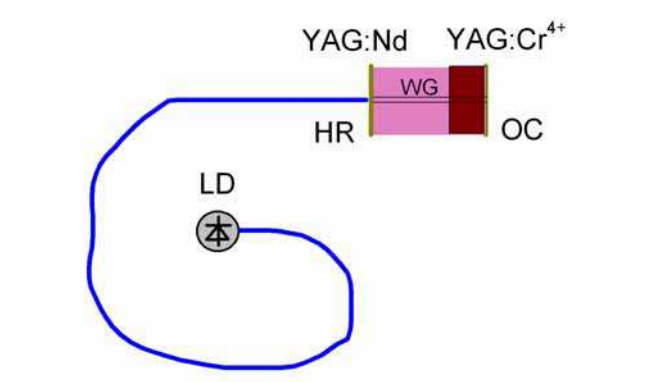

Fig. 21. Scheme of laser setup.

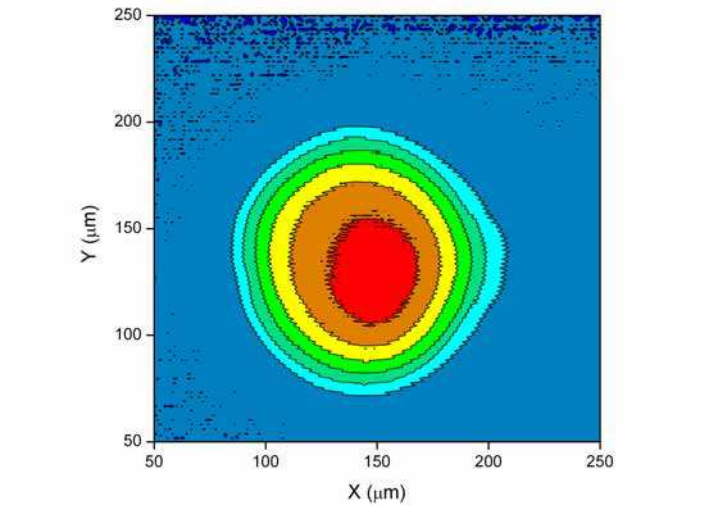

Fig. 22. Near field image of pump emission taken at OC location.

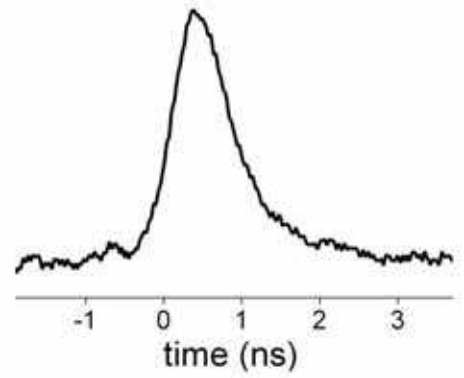

Fig. 23. Oscilloscope trace of a Q-switch pulse.

7. Conclusion

Micro-modification by means of femtosecond laser pulses is an effective tool for fabrication of low threshold and efficient waveguide lasers in YAG crystals. A beam with elliptical cross section is very effective tool for femtosecond inscription of depressed cladding waveguides in a low repetition rate regime. The technique is flexible for waveguide inscription with cross section of a predetermined shape. Both MPA and electron plasma absorptions are responsible for energy deposition and refractive index modification in YAG crystals. The presence of doping ions facilitates smart modification of crystal structure without optical damage and, as a result, refractive index change is not accompanied by disintegration of a crystal lattice during femtosecond laser inscription.

8. References

Allsop, T.; Dubov, M.; Mezentsev, V and Bennion, I. (2010), Inscription and characterization of waveguides written into borosilicate glass by a high-repetition-rate femtosecond laser at 800 nm. *Applied Optics*, Vol.49 (1938-1950).

Apostolopoulos, V.; Laversenne, L.; Colomb, T.; Depeursinge, C.; Salathé, R. P.; and Pollnau, M. (2004). Femtosecond-irradiation-induced refractive-index changes and channel waveguiding in bulk Ti^{3+}:Sapphire. *Appl. Phys. Lett.,* Vol. 85 (1122-1124).

Ashcroft, N.W. & Mermin, N.D. (1976). *Solid State Physics*, Holt, Rinehart, and Winston, New York.

Berg´e, L.; Skupin, S.; Nuter, R., Kasparian, J. and Wolf, J-P. (2007). Ultrashort filaments of light in weakly ionized, optically transparent media. *Rep. Prog. Phys*. Vol. 70 (1633–1713).

Bookey, H.T.; Thomson, R.R.; Psaila, N.D.; Kar, A.K.; Chiodo, N.; Osellame, R. and Cerullo, G. (2007). Femtosecond Laser Inscription of Low Insertion Loss Waveguides in Z-Cut Lithium Niobate. *IEEE Photonics Technology Letters*, Vol. 19 (892-894).

Burghoff, J.; Grebing, C.; Nolte, S. & Tunnermann, A. (2006). Efficient frequency doubling in femtosecond laser-written waveguides in lithium niobate. *Appl. Phys. Lett.,* Vol. 89 (081108).

Burghoff, J.; Hartung, H.; Nolte, S. & Tunnermann,A. (2007). Structural properties of femtosecond laser-induced modifications in $LiNbO_3$. *Appl. Phys. A*, Vol. 86 (165–170).

Davis, K.M.; Miura, K.; N. Sugimoto, N.; and Hirao, K. (1996), Writing waveguides in glass with a femtosecond laser. *Optics Letters*, Vol. 21 (1729-1731).

Dubov, M.V.; Krushchev, I.; Bennion, I.; Okhrimchuk, A. G. and Shestakov, A. V. (2004) Waveguide inscription in YAG:Cr^{4+} crystals by femtosecond laser irradiation, *in Conference on Lasers and Electro-Optics/International Quantum Electronics Conference and Photonic Applications Systems Technologies, Technical Digest (CD),* (Optical Society of America), paper CWA49.

Dubov, M.; Mezentsev, V. and Bennion, I. Femtosecond inscription of the first order bragg gratings in pure fused silica, (2006) in 2006 NSTI Nanotechnology Conference and Trade Show - NSTI Nanotech 2006 Technical Proceedings, Vol.3 (229–232), Nano Science and Technology Institute, (Boston, MA, United States of America).

Eaton, S.M.; Zhang, H.; Herman, P.R.; Yoshino, F.; Shah, L.; Bovatsek, J. & Arai, A. Y. (2005). Heat accumulation effects in femtosecond laser written waveguides with variable repetition rate. *Optics Express*, Vol. 13 (4708- 4716).

Feng, Q.; Moloney, J. V.; Newell, A. C.; Wright, E. M.; Cook, K.; Kennedy, P. K.; Hammer, D. X.; Rockwell, B. A. and Thompson, C. R. (1997). Theory and Simulation on the Threshold of Water Breakdown Induced by Focused Ultrashort Laser Pulses. *IEEE Journal of Quantum Electronics*, Vol. 33 (127-137).

Glezer, E.N. and Mazur, E. (1997). Ultrafast-laser driven micro-explosions in transparent materials. *Appl. Phys. Lett.,* Vol. 71 (882-884).

Gorelik, T.;Will, M.; Nolte,S.; Tuennermann,A. & Glatzel, U. (2003). Transmission electron microscopy studies of femtosecond laser induced modifications in quartz. *Appl. Phys. A*, Vol. 76 (309-311).

Guizard, S.; Martin, P. Daguzan, Ph; Petite; G.; Audeber, P.; Geindre, J. P.; Dos Santo, A. and Antonnett, A. (1995). Contrasted Behaviour of an Electron Gas in MgO, Al_2O_3 and SiO_2. *Europhys. Lett*., Vol. 29 (401-406).

Homoelle, D.; Wielandy, S.; Gaeta, A.L.; Borrelli, N. F. and Smith, C. (1999). Infrared photosensitivity in silica glasses exposed to femtosecond laser pulses. *Optics Letters*, Vol. 24 (1311-1313).

Kanehira, S.;_ Miura, K. and Hirao, K. (2008). Ion exchange in glass using femtosecond laser irradiation. *Appl. Phys. Lett.,* Vol. 93 (023112).

Landay, L.D. & Lifshits, E.M. (1982*) Theoretical Physics*, Vol.8, Nauka, Moscow (in Russian).

Lee, Y. L.;_ Yu, N. E.; Jung, C.; Yu, B.-A.; Sohn, I.-B.; Choi, S.-C.; Noh, Y.-C.; Ko, D.-K.; Yang, W.-S.; Lee, H.-M.; Kim, W.-K. and Lee, H.-Y. (2006). Second-harmonic generation in periodically poled lithium niobate waveguides fabricated by femtosecond laser pulses. *Appl. Phys. Lett.,* Vol. 89 (171103).

Liu, Y.; Zhu, B.; Wang, L.; Qiu, J.; Dai, Y. and Ma, H. (2008). Femtosecond laser induced coordination transformation and migration of ions in sodium borate glasses. *Appl. Phys. Lett.,* Vol. 92 (121113).

Liu, Y.; Shimizu, M.; Zhu, B.; Dai, Y.; Qian, B.; Qiu, J.; Shimotsuma, Y.; Miura, K. and Hirao K. (2009). Micromodification of element distribution in glass using femtosecond laser irradiation. *Optics Letters*, Vol. 34 (136-138).

Martin, P.; Guizard, S.; Daguzan, Ph.; Petite; G.; D'Oliveira, P.; Meynadier, P. and Perdrix, M. (1997-I). Subpicosecond study of carrier trapping dynamics in wide-band-gap crystals. *Phys. Rev. B*, Vol.55 (5799- 5809).

Miura, K.; Qiu, J.; Inouye, H.; Mitsuyu,T. & Hirao, K. (1997). Photowritten optical waveguides in various glasses with ultrashort pulse laser. *Appl. Phys. Lett.,* Vol. 71 (3329-3331).

Marshall, G.D.; Ams, M. and Withford, M.J. (2006). Direct laser written waveguide–Bragg gratings in bulk fused silica. *Optics Letters*, Vol. 31 (2690-2691).

Marshall, G.D.; Dekker, P.; Ams, M.; Piper, J.A. and Withford, M.J. (2008). Directly written monolithic waveguide laser incorporating a distributed feedback waveguide-Bragg grating. *Optics Letters*, Vol. 33 (956-958).

Moh, K.J.; Tan, Y.Y.; Yuan, X.-C.; Low, D.K.Y. & Li, Z.L. (2005). Influence of diffraction by a rectangular aperture on the aspect ratio of femtosecond direct-write waveguides. *Optics Express*, Vol. 13 (7288- 7297).

Nejadmalayeri, A.H.; Herman, P.R.; Burghoff, J.; Will, M.; Nolte, S. and Tünnermann, A. (2005). Inscription of optical waveguides in crystalline silicon by mid-infrared femtosecond laser pulses. *Optics Letters*, Vol. 30 (964-966).

Okhrimchuk, A.G.; Shestakov, A. V.; Khrushchev, I. and Mitchell, J. (2005 -a). Depressed cladding, buried waveguide laser formed in a YAG:Nd^{3+} crystal by femtosecond laser writing. *Optics Letters*, Vol. 30 (2248-2250).

Okhrimchuk, A.G.; Shestakov, A. V.; Khrushchev, I. & Bennion, I. (2005 -b). Waveguide Laser Inscribed in Neodimium YAG Crystal by Femtosecond Writing. TOPS V.98 (836-841), OSA, Ed. I. Sorokina and C. Denman, P.

Okhrimchuk, A.; Dubov, M.; Mezentsev, V. and Bennion, I. (2008). Permanent Refractive Index Change Caused by Femtosecond Laser Beam in YAG Crystals. *Proceedings of 3-d EPS-QEOD Europhoton conference,* TUp.15, Paris, France, August-September 2008.

Okhrimchuk, A.G.; Mezentsev, V.K.; Schmitz, H.; Dubov, M. and Bennion, I. (2009-a). Cascaded nonlinear absorption of femtosecond laser pulses in dielectrics", *Laser Physics*, Vol.19, (1415-1422).

Okhrimchuk, A.G.; Mezentsev, V.K.; Dvoyrin, V.V.; Kurkov, A.S.; Sholokhov, E.M.; Turitsyn, S.K.; Shestakov, A.V. and Bennion, I. (2009-b). Waveguide-saturable absorber fabricated by femtosecond pulses in YAG:Cr^{4+} crystal for Q-switched operation of Yb-fiber laser. *Optics Letters*, Vol. 34 (3881-3883).

Osellame, R.; Taccheo, S.; Marangoni, M.; Ramponi, R.; Laporta, P.; Polli, D.; De Silvestri, S. and Cerullo, G. (2003). Femtosecond writing of active optical waveguides with astigmatically shaped beams. *J. Opt. Soc. Am. B*, Vol.20 (1559-1567).

Schaffer, C.B.; Brodeur, A.; García, J.F. and Mazur, E. (2001). Micromachining bulk glass by use of femtosecond laser pulses with nanojoule energy. *Optics Letters*, Vol. 26 (93-95).

Siebenmorgen, J.; Petermann, K.; Huber, G.; Rademaker, K., Nolte, S. & Tünnermann, A. (2009). Femtosecond laser written stress-induced Nd:$Y_3Al_5O_{12}$ (Nd:YAG) channel waveguide laser. *Appl. Phys. B*, Vol. 97 (251–255).

Silva, W. F.; Jacinto, C.; Benayas, A.; Vazquez de Aldana, J. R.; Torchia, G. A.; Chen, F.; Tan, Y. and Jaque, D. (2010). Femtosecond-laser-written, stress-induced Nd:YVO_4 waveguides preserving fluorescence and Raman gain. *Optics Letters*, Vol. 35 (916-918).

Streltsov, A.M. and Borrelli, N.F. (2001). Fabrication and analysis of a directional coupler written in glass by nanojoule femtosecond laser pulses. *Optics Letters*, Vol. 26 (42-43).

Thomas, J.;_ Heinrich, M.; Burghoff, J.; Nolte, S.;. Ancona, A & Tünnermann, A. (2007). Femtosecond laser-written quasi-phase-matched waveguides in lithium niobate. *Appl. Phys. Lett.,* Vol. 91 (151108).

Torchia, G. A.;_ Rodenas, A.; Benayas, A.; Cantelar, E.; Roso, L. and Jaque, D. (2008). Highly efficient laser action in femtosecond-written Nd:yttrium aluminium garnet ceramic waveguides. *Appl. Phys. Lett.,* Vol. 92 (111103).

Turitsyn, S.K.; Mezentsev, V.K.; Dubov, M.; Rubenchik, A. M., Fedoruk, M. P. and Podivilov, E.V. (2007). Sub-critical regime of femtosecond inscription. *Optics Express*, Vol. 15 (14750-14764).

Qurerre, F.; Guizard, S. and Martin, Ph. (2001). Time-resolved study of laser-induced breakdown in dielectrics. *Europhys. Lett.*, Vol. 56 (138-144).

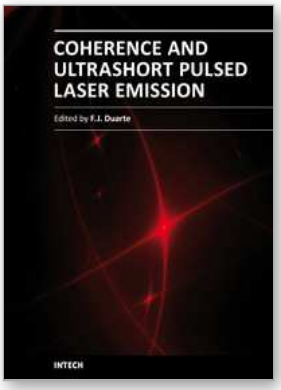

Coherence and Ultrashort Pulse Laser Emission

Edited by Dr. F. J. Duarte

ISBN 978-953-307-242-5
Hard cover, 688 pages
Publisher InTech
Published online 30, November, 2010
Published in print edition November, 2010

In this volume, recent contributions on coherence provide a useful perspective on the diversity of various coherent sources of emission and coherent related phenomena of current interest. These papers provide a preamble for a larger collection of contributions on ultrashort pulse laser generation and ultrashort pulse laser phenomena. Papers on ultrashort pulse phenomena include works on few cycle pulses, high-power generation, propagation in various media, to various applications of current interest. Undoubtedly, Coherence and Ultrashort Pulse Emission offers a rich and practical perspective on this rapidly evolving field.

InTech Europe
University Campus STeP Ri
Slavka Krautzeka 83/A
51000 Rijeka, Croatia
Phone: +385 (51) 770 447
Fax: +385 (51) 686 166
www.intechopen.com

InTech China
Unit 405, Office Block, Hotel Equatorial Shanghai
No.65, Yan An Road (West), Shanghai, 200040, China
中国上海市延安西路65号上海国际贵都大饭店办公楼405单元
Phone: +86-21-62489820
Fax: +86-21-62489821